2025 IEEE/SICE International Symposium on System Integration (SII)
January 21-24, 2025, Munich, Germany

Full Range Torque Estimation on Drivetrains with Strain Wave Gears*

Søren Graabæk[1,2] and Christoffer Sloth[1]

Abstract— **This paper consider sensorless joint torque estimation for kinesthetic teaching on industrial robots with strain wave gears. We show that a simple torsional compliance model of the gear can be used to augment the joint torque estimated by a generalized momentum observer to obtain accurate joint torque estimates when the system has zero momentum. This is accomplished by providing a framework for joining the two joint torque estimates and showing that the combined method has an improved Root Mean Square Error (RMSE) of 39%, as compared to the momentum observer, when the model parameters of the torsional compliance model are computed from the gear's datasheet and an improved Root Mean Square Error (RMSE) of 49% when the model parameters are estimated on data from the joint.**

I. Introduction

Code-free robot programming is an enabler for low-volume manufacturing to meet the increasing demand for customized products [1]. Kinesthetic teaching is a code-free robot programming approach that allows non-expert programmers to do robot programming by physically guiding an industrial robot with a collaborative teaching interface through a desired motion with their hands, see Fig. 1. The performance of a kinesthetic teaching interface depends on the robot's sensitivity to the user's applied forces. Poor sensitivity may lead to inaccurate demonstrations and excessive strain on the demonstrator. Improving the joint torque estimate can lead to better performance of the kinesthetic teaching interface. Therefore, in this paper, we study methods for estimating the joint torques on a Universal Robot (UR) robot. Specifically, we consider methods that only require data available from the built-in sensors in the UR joint.

Disturbance observers are typically used for torque estimation on industrial robots. At the same time, many industrial robots designed for human collaboration are built with strain wave gears. A strain wave gear consists of a *circular spline*, a *flexspline*, and a *wave generator* with a wave generator bearing. In drivetrains with strain wave gears, the torsional compliance can be used for torque estimation. Hence, torque estimation methods applicable for robots with strain wave gears can be divided into two types: torsional compliance approaches, and disturbance observer approaches.

The disturbance observer methods utilize a dynamic model of the joint to estimate the joint torque. The generalized momentum observer [2], [3], [4] is the most popular observer for external torque estimation because it does not rely on the joint's acceleration; this information is typically not available from measurements. The accuracy of the estimated torque depends on the quality of the underlying dynamical model. For joints with strain wave gears, the main model uncertainty is the friction, as it has been shown that the static friction is load- and direction-dependent; and that the viscous friction is nonlinearly dependent on the velocity, gear temperature, and teeth wear [5], [6], [7], [8]. However, even with a simple dynamic model, the momentum observer produces a good torque estimate. The drawback of the momentum observer is that it only produces valid torque estimates when the system has nonzero momentum. The drawback of the momentum observer is that it rely on a dynamic model that have high uncertainty at zero velocity due to friction, thus, it produces inaccurace torque estimates when the system have zero momentum. it only produces valid torque estimates when the system has nonzero momentum.

Fig. 1. Example of kinesthetic teaching on a UR5e robot.

The torsional compliance methods utilize the torsion measured by the encoder mounted on the input- and output-side of the gear and a model of the gear stiffness to estimate the joint torque. However, the torsion measurement is affected by kinematic error [9], [10] and hysteresis [11], [12], [13]. There is a general acceptance in the literature that the gear compliance stems from torsional deflection of the flexspline cup as well as deformation in the teeth engagement zone with the flexspline teeth being the softest component [14], [15]. Therefore, the loading and unloading stiffness curves are determined by the flexspline teeth stiffness. Deflection also occurs radially in the wave-generator bearing at low

*This work was supported by Innovation Fund Denmark [ref no. 1044-00187B] and Universal Robots A/S.

[1]SDU Robotics, University of Southern Denmark, Campusvej 55, 5220 Odense, Denmark {sggr,chsl}@mmmi.sdu.dk

[2]Universal Robots A/S, Energivej 51, 5260 Odense, Denmark sggr@universal-robots.com

torques due to the elasticity and clearance of the bearing race [16]; leading to a phenomenon called *lost motion*. By considering the compliance of the wave generator, the hysteresis behavior of the strain wave gear is captured without the need for a separate hysteresis model [17], [18] and, thereby, significantly reducing the complexity of the compliance method as compared to black-box methods such as the Maxwell-slip model [13].

We propose to merge the external torque estimated by a momentum observer with the external torque estimated by a compliance-based method to improve the joint torque sensitivity. Specifically, we propose to merge the momentum observer with the compliance model developed by [17] because the model parameters can be computed from generic values in the gear's datasheet and, thus, do not require training data measured on external hardware.

Many methods exist to merge sensor signals with noise, e.g., the Kalman filter, the complementary filter [19], [20] and the interacting multiple model (IMM) filter [21]. In this paper, we use the concepts from the IMM filter and treat the two torque estimates as a split range sensor. I.e., we assume that the torque estimated by the momentum observer is valid when the system is in motion and that the torque estimated by the compliance method is valid when the system is at standstill. Hence, we need to design a switching function to merge the two estimates.

The contribution of this paper is to identify the methods' performance in motion and no motion. And show that the overall torque estimate can be improved if we consider different methods for the two scenarios.

This paper is organized as follows. In Section II we present our proposed merged torque method along with the generalized momentum observer and the compliance model. In Section III we present the experimental setup and the validation dataset used to compare the methods, followed by Section IV where we present the result of this paper. Lastly, Section V concludes the paper.

II. Torque Estimation Methods

The UR joint consists of a strain wave gear supported by a cross roller bearing and two support bearings, and a motor mounted on the gear shaft, as illustrated in Fig. 2. The joint is equipped with an encoder measuring the input-side position, θ; an encoder measuring the output-side position, q; and an ammeter measuring the input current to the motor. For simplicity, we assume that the motor dynamics are known and, thus, that we measure the motor torque τ_m. The gear ratio is given by $N = z_f/(z_c - z_f)$, where z_f and z_c are the number of flexspline teeth and circular spline teeth, respectively. The gear is configured with the wave generator as the input, the circular spline as the output, and the flexspline mounted to the joint house, i.e., the acceleration of the flexspline in zero, which gives an effective gear ratio of $\tilde{N} = N + 1$.

A. Disturbance Observer

A lumped mass diagram of the joint is illustrated in Fig. 3. Different gear models can be inserted to create a dynamic

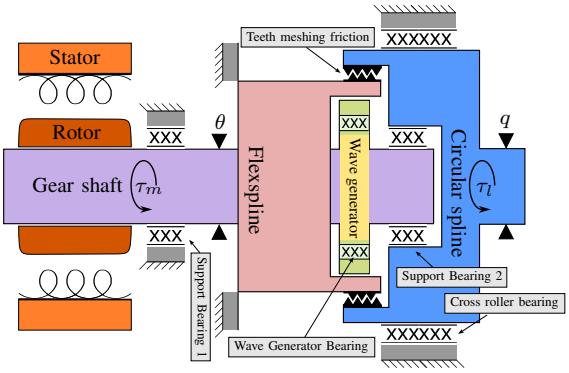

Fig. 2. Schematic of an UR e-seires joint illustrating the interaction between the strain wave gear components, the motor, and the joint bearings.

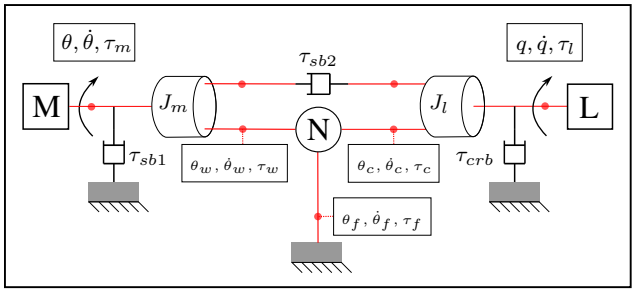

Fig. 3. A lumped mass diagram of a robot joint. The joint consist of three bearings with friction torque τ_{sb1}, τ_{sb2}, and τ_{crb}; a motor with position θ generating a torque τ_m; a load with position q generating a torque τ_l; and a strain wave gear with a wave generator-, circular spline- and flexspline-side with position and torque denoted by the subscript w, c and f, respectively.

model of the joint. In this paper, we assume that the gear is rigid with the gear equation given by [5, Model 2]:

$$\theta_w = \theta_c \tilde{N}, \quad \tau_w = \frac{\tau_c + \tau_{fric}}{\tilde{N}}, \tag{1}$$

where $\tau_{fric} \in \mathbb{R}$ is the aggregated friction torque; $\theta_w, \tau_w \in \mathbb{R}$ and $\theta_c, \tau_c \in \mathbb{R}$ is the position and torque at the wave generator- and circular spline-side of the gear, respectively. Futhermore, we assume that the rotor is cylindrical with its center of mass aligned with the shaft axis, i.e., the gravitational potential energies of the joint is independent of the rotor position [22]. Thus, we derive the following dynamic equation:

$$J\ddot{q} + C(q, \dot{q})\dot{q} + \tau_{fric}(\dot{q}) + g(q) = \tau_m \tilde{N} - \tau_l - \tau_d, \tag{2}$$

where $J \in \mathbb{R}$ is the joint inartia; $C \in \mathbb{R}$ contains the Coriolis and centrifugal terms; $g \in \mathbb{R}$ is the torque resulting from gravity; $\tau_m \in \mathbb{R}$ is the motor torques; $\tau_l \in \mathbb{R}$ is the known load torque at the output flange; and $\tau_d \in \mathbb{R}$ are the unknown disturbance torques.

In the following, we utilize the joint dynamic equation in (2) to design a generalized momentum observer, see [2] for details. The generalized momentum p of a mechanical system is:

$$p = J\dot{q}. \tag{3}$$

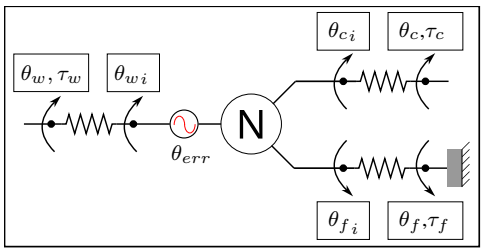

Fig. 4. Kinematic representation of the compliance model for the strain wave gear. θ_w, θ_c and θ_f denote the wave generator-, circular spline- and flexspline-side position, respectively, and the additional subscript i denote the position of the internal side of the spring. θ_{err} is the kinematic error.

Comparing the predicted generalized momentum with the measured generalized momentum, a disturbance torque can be estimated. To design the generalized momentum observer, we compute the time-derivative of the generalized momentum:

$$\dot{p} = \dot{J}\dot{q} + J\ddot{q}. \tag{4}$$

Inserting (2) into (4), we obtain:

$$\dot{p} = \dot{J}\dot{q} + \tau_m\tilde{N} - \tau_l - \tau_d - C(q,\dot{q})\dot{q} - \tau_{fric}(\dot{q}) - g(q). \tag{5}$$

Since $\dot{J} = C(q,\dot{q}) + C^T(q,\dot{q})$, we get:

$$\dot{p} = \underbrace{\tau_m\tilde{N} - \tau_l + C^T(q,\dot{q})\dot{q} - \tau_{fric}(\dot{q}) - g(q)}_{=\bar{\tau}} - \tau_d. \tag{6}$$

An observer for the generalized momentum is:

$$\dot{\hat{p}} = \bar{\tau} + L(p - \hat{p}), \tag{7}$$

where L is the observer gain, which can be chosen to obtain a desired rate of convergence. Finally, assuming that the disturbance torque τ_d is the torque applied by the user, the external torque can be estimated as:

$$\hat{\tau}_e = -L(p - \hat{p}). \tag{8}$$

B. Torsional Compliance Method

In this paper we use the compliance method developed in [17] because the model parameters, except the kinematic error, can be estimated from the datasheet of the gear. The method assumes that the gear consist of two compliant component: the wave generator and the teeth meshing zone; the modelled kinematic representation of the gear is shown in Fig. 4. Note that the meshing stiffness can be seen from both the circular spline and flexspline port, but the deflection at the flexspline will be invisible due to the gear configuration.

To derive the model we first define the torsion across the wave generator and the teeth meshing zone:

$$\Delta\theta_w = \theta_{wi} - \theta_w \tag{9}$$

$$\Delta\theta_m = \theta_c - \theta_{ci}, \tag{10}$$

where θ_{wi} and θ_{ci} are internal gear positions that cannot be measured. However, we can measure the joint torsion:

$$\Delta\theta = q\tilde{N} - \theta = \theta_c\tilde{N} - \theta_w, \tag{11}$$

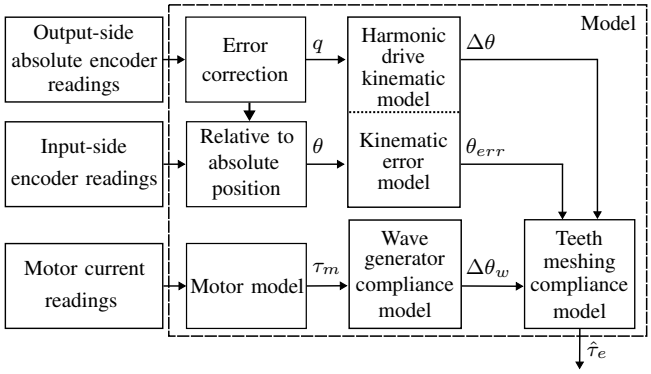

Fig. 5. Block diagram of the implemented compliance method.

and from Fig. 4, we have the following kinematic contraint across the gear:

$$\theta_{ci}\tilde{N} = \theta_{wi} + \theta_{err}, \tag{12}$$

where θ_{err} is the kinematic error. By adding and subtracting θ_{wi} and $\theta_{ci}\tilde{N}$ in (11), we get the following relation between the torsion measurement, the kinematic error and the deflection of the wave generator and teeth meshing zone:

$$\Delta\theta = (\theta_{wi} - \theta_w) + (\theta_c - \theta_{ci})\tilde{N} + (\theta_{ci}\tilde{N} - \theta_{wi}) \tag{13}$$

$$= \Delta\theta_w + \Delta\theta_m\tilde{N} + \theta_{err}. \tag{14}$$

To use (14) for estimating the external torque, we need to derive a relation between the deflection and the torque. From [17], we know that the deflection of the teeth meshing zone can be related to the circular spline torque as:

$$\Delta\theta_m = \frac{\operatorname{atan}(c_c\tau_c)}{c_cK_{c0}}, \tag{15}$$

and that the deflection of the wave generator can be related to the motor torque as:

$$\Delta\theta_w = \frac{\operatorname{sgn}(\tau_m)}{c_wK_{w0}}\left(1 - e^{-c_w|\tau_m|}\right), \tag{16}$$

where K_{m0}, c_m, K_{w0} and c_w are constants to be determined. The external torque can be estimated as:

$$\hat{\tau}_e = \tau_c - \tau_l, \tag{17}$$

where τ_c is computed as:

$$\tau_c = \frac{\tan(\Delta\theta_m c_m K_{m0})}{c_m}. \tag{18}$$

A block diagram of the method is shown in Fig. 5.

C. Merged Torque Method

When switching between the two estimated torque signals, it is necessary to make a smooth transition to guarantee a reliable output of the estimation method. Hence, we use a convex combination of the estimates in the transition period:

$$\hat{\tau}_{e,m} = \lambda(\dot{q}) \cdot \hat{\tau}_{e,o} + (1 - \lambda(\dot{q})) \cdot \hat{\tau}_{e,c}, \tag{19}$$

where $\hat{\tau}_{e,o}$ is the external torque estimated by the momentum observer; $\hat{\tau}_{e,c}$ is the external torque estimate by the compliance model; $\hat{\tau}_{e,m}$ is the merged signal; and $\lambda(\dot{q}) \in [0,1]$

Fig. 6. Test setup with a standalone UR joint with a force/torque sensor and a pulley system mounted on the output flange.

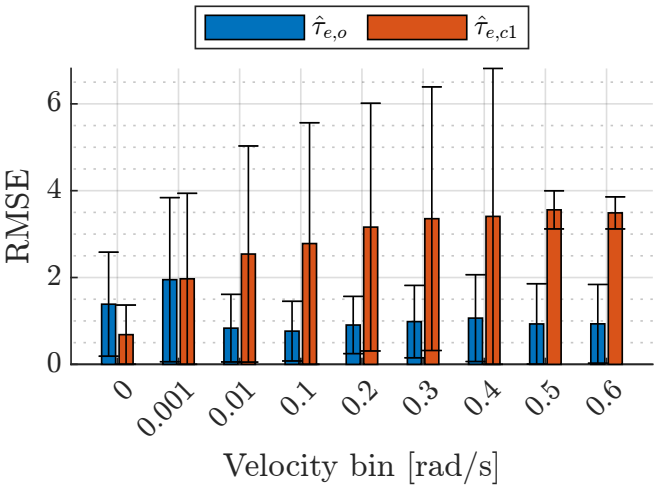

Fig. 7. RMSE value (with standard deviation) of the torque estimation error vs velocity for the momentum observer $\hat{\tau}_{e,o}$ and the compliance model $\hat{\tau}_{e,c1}$ as measured on the trainings dataset.

is the transition function. In this paper, we use the logistic function as the transition function:

$$\lambda(\dot{q}) = \frac{1}{1 + e^{-\alpha(|\dot{q}| - \dot{q}_{trans})}} \tag{20}$$

where $\dot{q}_{trans}$ is the velocity at which the signals will be equally mixed, and α determine the transition slope.

III. Experimental Setup

In this section, we present the experiment used to generate data to compare the torque estimation methods. The setup consists of a standalone UR joint size 2.5 with a UR force/torque sensor and a pulley system. A photo of the setup is shown in Fig. 6. The joint is controlled using a UR control box with custom-built firmware that enables direct control of the motor current and input-side velocity. The motor torque, τ_m, the external torque, τ_e, and the raw input- and output-side position, θ and q, are sampled by a custom-built data interface to guarantee data alignment. All measurements are resampled to 500 Hz.

To compare the methods, a validation dataset is recorded with an external torque manually applied to the pulley disc

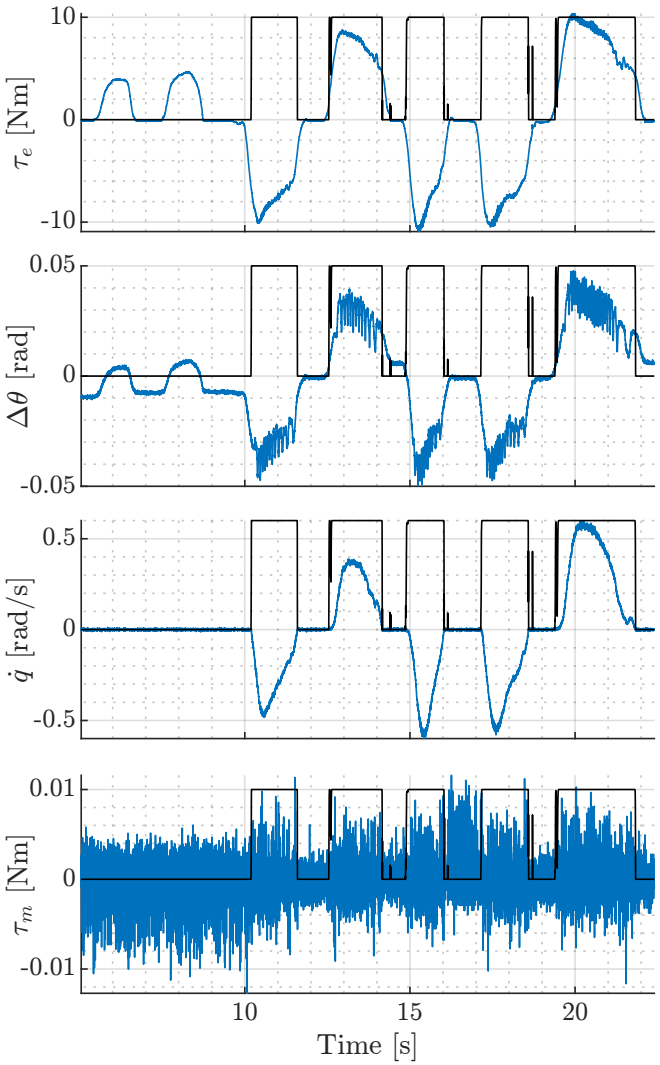

Fig. 8. Subset of the validation dataset. The black line is the transition function $\lambda(\dot{q})$ scaled to the displayed signal amplitude: 0 indicate *no motion* and a high signal indicate *motion*; τ_e is the measured external torque; $\Delta\theta$ is the measured torsion; $\dot{q}$ is the output-side velocity; and τ_m is the motor torque.

while the motor current is commanded to zero. The external torque is applied in the following two ways:

1) **Motion**: The external torque is large and backdrives the joint.
2) **No motion**: The external torque is small and does not backdrive the joint, but a joint deflection is observed.

A subset of the dataset is shown in Fig. 8.

IV. Results

In this section, we present the Root Mean Square Error (RMSE) and error variance of a selection of torque estimation methods together with our proposed merged torque method.

The momentum observer is implemented as a discrete time system with gain $L_d = -8$ and the model parameters of the underlying dynamic model are estimated on a training dataset as described in [5, Model 2]. The torque estimated

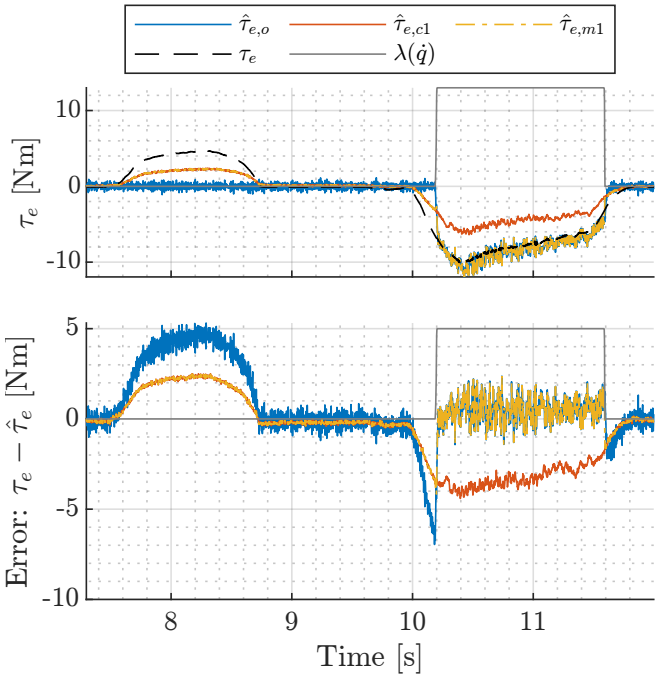

Fig. 9. The estimated external torque on a subset of the validation dataset. $\hat{\tau}_{e,o}$ is the torque estimated by momentum observer; $\hat{\tau}_{e,c1}$ is the torque estimated by the compliance model with parameters computed based on the gear's datasheet; and $\hat{\tau}_{e,m1}$ is the result of merging the two estimates.

TABLE I
RMSE AND (ERROR VARIANCE) OF IMPLEMENTED TORQUE ESTIMATION METHODS ON THE VALIDATION DATASET.

		Full	Motion	No motion
Ours	$\hat{\tau}_{e,m1}$	1.03 (1.06)	1.01 (0.98)	1.04 (1.07)
	$\hat{\tau}_{e,m2}$	0.87 (0.75)	1.02 (1.05)	0.74 (0.55)
Momentum observers	$\hat{\tau}_{e,o}$	1.69 (2.85)	1.01 (0.99)	2.03 (4.10)
Compliance models	$\hat{\tau}_{e,c1}$	2.24 (4.99)	3.24 (10.44)	1.09 (1.19)
	$\hat{\tau}_{e,c2}$	1.02 (1.02)	1.33 (1.67)	0.74 (0.55)
	$\hat{\tau}_{e,sd}$	1.23 (0.54)	1.30 (0.47)	1.17 (0.57)
	$\hat{\tau}_{e,gp}$	1.62 (2.61)	1.54 (2.35)	1.67 (2.79)

by the momentum observer is denoted by $\hat{\tau}_{e,o}$ and the model parameters are shown in Appendix. Two sets of model parameters are used for the torsional compliance method in Section II-B: For both parameter sets, the kinematic error is estimated on a training set, as described in [5, Model 4]; for the first set, the stiffness coefficients are computed from the stiffness curve in the gear's datasheet, as in [17]; and for the second set, the stiffness coefficients are computed from the stiffness curve measured on the joint. Both parameter sets are shown in the Appendix. The torque estimated by the first and second set of parameters is denoted by $\hat{\tau}_{e,c1}$ and $\hat{\tau}_{e,c2}$, respectively. Lastly, $\hat{\tau}_{e,m1}$ and $\hat{\tau}_{e,m2}$ denotes the torque estimated by the merged model utilizing the first and second set of compliance model parameters, respectively. The model parameters α and $\dot{q}_{trans}$ are selected to give the lowest RMSE value on the estimated torque on the training dataset, see Fig 7 for a visualization of the error for different velocity bins. The model parameters are found to be $\alpha = 500$ for both models, and $\dot{q}_{trans} = 0.001$ and $\dot{q}_{trans} = 0.45$ for $\hat{\tau}_{e,m1}$ and $\hat{\tau}_{e,m2}$, respectively. Figure 9 vizualize $\hat{\tau}_{e,m1}$ together with $\hat{\tau}_{e,o}$ and $\hat{\tau}_{e,c1}$.

Table I show the RMSE, and error variance, of the estimated torques on the validation dataset together with the external torque estimated by: $\hat{\tau}_{e,sd}$, a structural damping model developed in [23]; and $\hat{\tau}_{e,gp}$, a Gaussian Process model trained on the input variables $[q, \theta, \dot{q}, \theta, \tau_m]$ on a training dataset similar to the validation dataset with 22070 samples. In Table I, we see that the RMSE values for the compliance-based methods are lower than the RMSE for the momentum observer when the system has zero momentum, and vice versa. Therefore, we also see an improved full-range RMSE value for the merged models; 39% and 49% improvement for $\hat{\tau}_{e,m1}$ and $\hat{\tau}_{e,m2}$, respectively. I.e., we see an improvement of the RMSE value for the merged method regardless of whether the compliance model is computed from the datasheet values or a training dataset.

V. Conclusion

In this paper, we showed that the compliance of a strain wave gear, mounted inside a robot joint, can be used to improve the RMSE value of the external torque estimated by a generalized momentum observer. Specifically, we showed that, for our dataset, the RMSE value can be improved by up to 49% when a compliance-based method is used to estimate the external torque when the system has zero momentum. Additionally, this paper showed that the improvement can be achieved, even when the compliance-based model parameters are computed from generic values in the gear's datasheet.

APPENDIX

This appendix provide the model paremeter used by the momentum observer and the compliance model.

A. Momentum Observer

Table II show the model parameters for the dynamic model in (2). We use a third order polynomial to model the friction torque [5]:

$$\tau_{fric} = \text{sgn}(\dot{q}) \left[f_C + f_{v,1} |\dot{q}| + f_{v,2} |\dot{q}|^2 + f_{v,3} |\dot{q}|^3 \right], \quad (21)$$

and the Coulomb friction is selected based on the joint's moving direction:

$$f_C = \begin{cases} f_{C-}, & \text{if } \text{sgn}\, \dot{q} < 0 \\ f_{C+}, & \text{otherwise,} \end{cases} \quad (22)$$

B. Compliance Model

Table II shows the parameters for the compliance model in (17) and the constants are computed as in [17]. The kinematic error is modelled as:

$$\theta_{err} = \sum_{i=1}^{k} a_i \cos\left(\omega_i \cdot q + \varphi_i\right), \quad (23)$$

where k is the number of frequency components; ω is the signal frequency; a is the signal amplitude; and φ is the signal phase offset.

TABLE II

MODEL PARAMETERS FOR THE MOMENTUM OBSERVER.

Name		Unit	$\hat{\tau}_{e,o}$
Observer gain*	L_d	[ ]	80
Gear ration	N	[ ]	100
Inertia	J	[Kg·m^2]	1.9221
Coriolis	C	[Nm·rad·s^{-1}]	0.0
Gravity	g	[Nm]	0.0
Joint load	τ_l	[Nm]	0.0
Coulomb friction			
- negative	f_{C-}	[Nm]	5.7429
- positive	f_{C+}	[Nm]	5.1586
Viscous friction			
- coefficient v	$f_{v,1}$	[Nm·(rad·s^{-1})$^{-1}$]	10.3207
- coefficient v^2	$f_{v,2}$	[Nm·(rad·s^{-1})$^{-2}$]	-5.1580
- coefficient v^3	$f_{v,3}$	[Nm·(rad·s^{-1})$^{-3}$]	1.2135

*Discrete time gain.

TABLE III

MODEL PARAMETER FOR THE COMPLIANCE MODELS.

Name		Unit	$\hat{\tau}_{e,c1}$	$\hat{\tau}_{e,c2}$
Gear ration	N	[ ]	100	100
Meshing zone constants				
- stiffness	$K_{m,0}$	[Nm·rad]	**15548**	**26431**
-	c_m	[Nm^{-1}]	0.0487	0.0487
Wave generator constant				
- stiffness	$K_{w,0}$	[Nm·rad]	21.9931	21.9931
-	c_w	[Nm^{-1}]	3.1250	3.1250
Kinematic error				
- ω_0 = 1, φ_0 = -0.9089	a_0	[mrad]	0.5725	0.5725
- ω_1 = 2, φ_1 = 1.7965	a_1	[mrad]	3.0897	3.0897
- ω_2 = 4, φ_2 = -1.3968	a_2	[mrad]	2.5476	2.5476
- ω_3 = 100, φ_3 = -0.9092	a_3	[mrad]	0.4770	0.4770
- ω_4 = 101, φ_4 = -1.2547	a_4	[mrad]	0.1289	0.1289
- ω_5 = 200, φ_5 = 2.2575	a_5	[mrad]	4.3530	4.3530
- ω_6 = 201, φ_6 = -2.5073	a_6	[mrad]	0.6327	0.6327
- ω_7 = 202, φ_7 = 1.7018	a_7	[mrad]	0.7937	0.7937
- ω_8 = 400, φ_8 = 0.8252	a_8	[mrad]	2.3372	2.3372
- ω_9 = 404, φ_9 = 0.9262	a_9	[mrad]	0.1693	0.1693

REFERENCES

[1] SPARC, "Strategic research agenda for robotics in Europa 2014-2022," 2014, accessed: 2023-04-11.

[2] A. De Luca and R. Mattone, "Sensorless robot collision detection and hybrid force/motion control," in *Proceedings of the 2005 IEEE international conference on robotics and automation*, 2005, pp. 999–1004.

[3] A. Mohammadi, H. J. Marquez, and M. Tavakoli, "Nonlinear disturbance observers: Design and applications to Euler-Lagrange systems," *IEEE Control Systems Magazine*, vol. 37, no. 4, pp. 50–72, 2017.

[4] G. Evangelisti and S. Hirche, "Data-driven momentum observers with physically consistent Gaussian processes," *IEEE Transactions on Robotics*, 2024.

[5] T. D. Tuttle, "Understanding and modeling the behavior of a harmonic drive gear transmission," *NASA STI/Recon Technical Report N*, vol. 93, p. 24152, 1992.

[6] H. D. Taghirad, "On the modeling and identification of harmonic drive systems," *Tech. Rep. CIM-TR-97-02, McGill Univ., Centre for Intelligent Machines*, 1997.

[7] E. Madsen, O. S. Rosenlund, D. Brandt, and X. Zhang, "Comprehensive modeling and identification of nonlinear joint dynamics for collaborative industrial robot manipulators," *Control Engineering Practice*, vol. 101, p. 104462, 2020.

[8] S. Graabæk, N. K. Poulsen, and C. Sloth, "Dynamics modeling of robot joints with asymmetric load-dependent friction," *IFAC-PapersOnLine*, vol. 58, no. 15, pp. 43–48, 2024.

[9] F. H. Ghorbel, P. S. Gandhi, and F. Alpeter, "On the kinematic error in harmonic drive gears," *Journal of Mechanical Design*, vol. 123, no. 1, pp. 90–97, 2001.

[10] H. Jia, J. Li, G. Xiang, J. Wang, K. Xiao, and Y. Han, "Modeling and analysis of pure kinematic error in harmonic drive," *Mechanism and Machine Theory*, vol. 155, p. 104122, 2021.

[11] R. Dhaouadi, F. H. Ghorbel, and P. S. Gandhi, "A new dynamic model of hysteresis in harmonic drives," *IEEE Transactions on Industrial electronics*, vol. 50, no. 6, pp. 1165–1171, 2003.

[12] C. Preissner, T. Royston, and D. Shu, "A high-fidelity harmonic drive model," *Journal of Dynamic Systems, Measurement, and Control*, vol. 134, pp. 011 002–13, 2012.

[13] T. Tjahjowidodo, F. Al-Bender, and H. Van Brussel, "Theoretical modelling and experimental identification of nonlinear torsional behaviour in harmonic drives," *Mechatronics*, vol. 23, no. 5, pp. 497–504, 2013.

[14] J. Ma, C. Li, Y. Luo, and L. Cui, "Simulation of meshing characteristics of harmonic reducer and experimental verification," *Advances in Mechanical Engineering*, vol. 10, no. 3, 2018.

[15] T. Tang, H. Jia, J. Li, J. Wang, and X. Zeng, "Modeling of transmission compliance and hysteresis considering degradation in a harmonic drive," *Applied Sciences*, vol. 11, no. 2, p. 665, 2021.

[16] N. Kircanski, A. A. Goldenberg, and S. Jia, "An experimental study of nonlinear stiffness, hysteresis, and friction effects in robot joints with harmonic drives and torque sensors," in *Experimental Robotics III: The 3rd International Symposium*, 2005, pp. 326–340.

[17] H. Zhang, S. Ahmad, and G. Liu, "Modeling of torsional compliance and hysteresis behaviors in harmonic drives," *IEEE/ASME Transactions on Mechatronics*, vol. 20, no. 1, pp. 178–185, 2014.

[18] Z. Shi, Y. Li, and G. Liu, "Adaptive torque estimation of robot joint with harmonic drive transmission," *Mechanical Systems and Signal Processing*, vol. 96, pp. 1–15, 2017.

[19] S. Särkkä and L. Svensson, *Bayesian filtering and smoothing*. Cambridge university press, 2023, vol. 17.

[20] W. T. Higgins, "A comparison of complementary and Kalman filtering," *IEEE Transactions on Aerospace and Electronic Systems*, no. 3, pp. 321–325, 1975.

[21] E. Mazor, A. Averbuch, Y. Bar-Shalom, and J. Dayan, "Interacting multiple model methods in target tracking: a survey," *IEEE Transactions on aerospace and electronic systems*, vol. 34, no. 1, pp. 103–123, 1998.

[22] M. W. Spong, "Modeling and control of elastic joint robots," *Journal of Dynamic Systems, Measurement, and Control*, vol. 109, no. 4, pp. 310–318, 1987.

[23] M. A. Ismail, J. Windelberg, and G. Liu, "Simplified sensorless torque estimation method for harmonic drive based electro-mechanical actuator," *IEEE Robotics and Automation Letters*, vol. 6, no. 2, pp. 835–840, 2021.